JEEEIT TRANSACTIONS, Vol.03,No.01,July 2026

Adaptive Smith Predictor with Resonance Compensation for Time-Delayed Lightly-Damped Systems

Aleisawee Mohamed Alsseid*[1], Nehal A. Alsseid[1], Abdulnasir S. Alfirjani[1]

[1]Control Engineering Department, College of Electronic Technology, Bani Walid, Libya

Corresponding author: dr.Aleisawee@gmail.com

ABSTRACT Time delays and mechanical resonance frequently coexist in industrial servo systems such as robotic manipulators, high-speed servos, and active magnetic bearings (AMBs). This paper presents an Adaptive Smith Predictor with Resonance Compensator (ASP-NRC) that simultaneously addresses both challenges. The architecture integrates: (i) a full-gain Smith predictor ($\lambda_s = 1$) with a correctly implemented causal fractional-delay FIR filter whose bulk delay is explicitly separated; (ii) a series adaptive notch filter whose zeros cancel the plant poles and whose pole Q-factor is adapted via an envelope-based scheduler; and (iii) a rigorous modular stability analysis establishing uniform ultimate boundedness (UUB) of all closed-loop signals. Extensive simulations over six benchmark cases with Monte Carlo trials, colored noise, robustness to resonance-frequency mismatch, and severe simultaneous parameter uncertainties show that ASP-NRC outperforms PID, Smith predictor, and Smith + fixed-notch controllers. For the nominal case, ASP-NRC achieves 98.1% ISE reduction versus PID and maintains > 5 dB resonance suppression for frequency mismatches up to $\pm 5\%$. Under ideal parameter matching, suppression reaches $S_{dB} = -85.18$ dB (i.e., 85.18 dB effective suppression) at the resonance frequency. The controller remains stable under severe combined uncertainties ($\pm 20\%$ on all parameters).

KEYWORDS Adaptive control, Fractional-delay FIR filter Smith predictor, Gain scheduling, Notch filters, Mechatronic systems, LPV systems.

I. INTRODUCTION

Industrial control systems often suffer from two detrimental phenomena: time delays from communication and sensing, and mechanical resonance caused by flexible modes. When both are present—as in robotic manipulators, high-speed servos, and active magnetic bearings (AMBs)—conventional controllers face a dilemma: high-gain feedback for tracking can destabilize due to delay-induced phase lag, while the same control action excites resonant modes. These applications demand precise positioning and disturbance rejection, making the simultaneous compensation of delay and resonance a critical practical problem.

The Smith predictor [1] remains the standard for dead-time compensation, with variants including filtered [2], two-degree-of-freedom [3], and data-driven designs [4]. Adaptive extensions for time-varying delays [5] and Lyapunov-based improvements [6] have been reported, as have sliding-mode [13] and active-disturbance-rejection [14] variants. For resonance suppression, positive position feedback (PPF) and its adaptive variant (APPF) [7], [8], are effective, with recent extensions to delayed systems [9], [15] and exact H_∞ tuning [10]. Hybrid approaches combining Smith predictors with fixed notch filters exist [11], [12], but they typically lack adaptation. Repetitive controllers with fractional delay have also been explored [16]. Neuro-fuzzy approaches have also been proposed for Smith predictor tuning [28].

Notably, Liu et al. [12] employ adaptive notch filters in servo systems; however, their approach tunes notch parameters via frequency-scanning heuristics rather than an envelope-based scheduler, and the notch is placed in a feedback path rather than in series with the controller output. The proposed ASP-NRC differs fundamentally: it integrates the adaptive notch within a Smith predictor architecture, uses an analytically predictable envelope-driven Q-factor scheduler, and places the notch in series to ensure resonance suppression is independent of controller gain. This series placement, combined with inverse PID gain scheduling, yields a modular design with explicit stability certificates.

The key contributions of this paper are:

1. A full-gain Smith predictor ($\lambda_s = 1$) with a correctly implemented causal fractional-delay

FIR filter. The integer and fractional parts of the delay are handled separately, ensuring the model delay equals the plant delay exactly with no non-causal “compensation.”

2. A series adaptive notch filter whose zeros are placed at the plant’s resonant poles. The pole Q-factor is adapted by an envelope-based scheduler, yielding an analytically predictable notch depth.

3. A modular stability analysis that treats the delay-compensated loop (small-gain theorem), the gain-scheduled dynamics (LPV gridding with explicit LMI certificates), and the nonlinear adaptation bounds (UUB), together with an honest discussion of the interconnection limitations.

4. Comprehensive simulation validation across six benchmark cases, including a 50-run Monte Carlo study, resonance-frequency mismatch robustness analysis, and severe combined uncertainty tests (±20%), all performed with a unified simulation framework.

II. Problem Formulation

2.1 System Description

We consider the canonical second-order-plus-delay model:

$$G(s) = \frac{K\omega_n^2}{s^2+2\zeta\omega_n s+\omega_n^2} e^{-\tau s} \tag{1}$$

With state-space representation: $\dot{x}_1 = x_2$

$$\dot{x}_2 = -2\zeta\omega_n x_2 - \omega_n^2 x_1 + K\omega_n^2 u(t-\tau) \tag{2}$$

$y = x_1$

Nominal parameters (Case A): $K = 1.5$, $\omega_n = 12.57$ rad/s (2.0 Hz), $\zeta = 0.05$ ($Q_{plant} = 1/(2\zeta) = 10$), $\tau = 0.150$ s, $T_s = 0.001$ s.

2.2 Control Objectives

The reference signal is defined as a unit step applied at $t = 2$ s:

$$r(t) = \begin{cases} 0 & t < 2\text{ s} \\ 1 & t \geq 2\text{ s} \end{cases} \tag{3}$$

Performance metrics (evaluated over [5,25] s):

$$ISE = \int_5^{25} [r(t) - y(t)]^2\, dt \tag{4}$$

$$IAE = \int_5^{25} |r(t) - y(t)|\, dt \tag{5}$$

$$S_{dB} = 10\log_{10}\left(\frac{P_{ASP}}{P_{PID}}\right) \text{ at } \omega = \omega_n \tag{6}$$

where P denotes the closed-loop power-spectral density obtained via swept-sine simulation. Additional metrics include control effort $\int |u|\, dt$, peak control rate $\| \dot{u} \|_\infty$, and settling time (2% band). The suppression metric S_{dB} uses a negative sign convention: a negative value indicates that ASP-NRC achieves lower resonance power than PID (i.e., effective suppression), while a positive value indicates amplification.

III. ASP-NRC Architecture

3.1 Overview

The ASP-NRC architecture comprises three cascaded layers, as illustrated in Fig. 1. Layer 1 is a full-gain Smith predictor with a causal fractional-delay FIR filter that exactly compensates for the plant time delay. Layer 2 is a series adaptive notch filter whose Q-factor is scheduled by an envelope detector driven by the predicted output. Layer 3 is a gain-scheduled PID controller with anti-windup compensation. The modular structure allows independent analysis of the delay-compensated loop, the LPV gain-scheduled dynamics, and the nonlinear adaptation bounds.

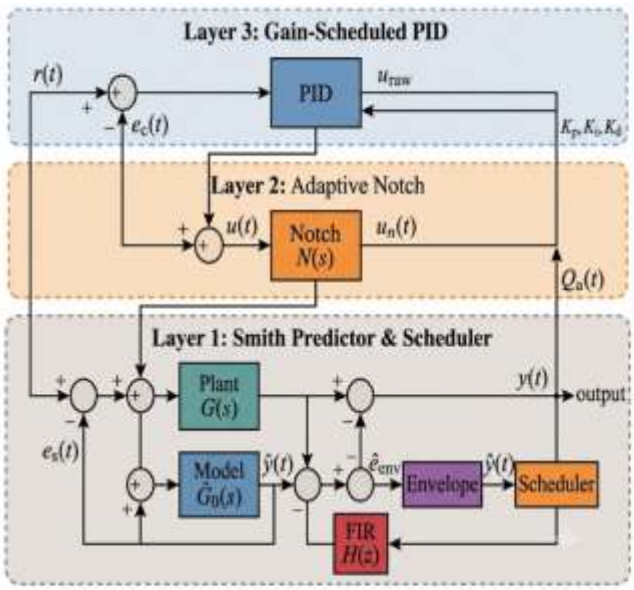

FIGURE 1. ASP-NRC architecture block diagram. Layer 1: full-gain Smith predictor with causal fractional-delay FIR filter. Layer 2: series adaptive notch filter with envelope-based Q-factor scheduling. Layer 3: gain-scheduled PID with anti-windup.

3.2 Layer 1: Full-Gain Smith Predictor with Fractional Delay

3.2.1 Nominal Model

The delay-free nominal model predicts the undelayed output $\hat{y}(t)$:

$$\begin{aligned} \dot{\hat{x}}_1 &= \hat{x}_2, \\ \dot{\hat{x}}_2 &= -2\zeta\omega_n\hat{x}_2 - \omega_n^2\hat{x}_1 + K\omega_n^2 u_n(t) \\ \hat{y} &= \hat{x}_1. \end{aligned} \tag{7}$$

Here $u_n(t)$ is the notched control signal defined in Section 3.3, so that $\hat{y}(t) = \hat{G}_0(s)N(s)u(t)$. The parameter λ_s denotes the predictor feedback gain; with $\lambda_s = 1$, the full correction is applied, removing the delay from the closed-loop characteristic equation exactly. The envelope detector operates on $\hat{y}(t)$ rather than $y(t)$ to avoid introducing the plant delay into the adaptation loop.

3.2.2 Fractional Delay Filter with Separated Bulk Delay

For $\tau = nT_s + \tau_f$ with $n = \lfloor \tau/T_s \rfloor$ and $0 \le \tau_f < T_s$, we decompose the delay into an integer bulk delay and a fractional interpolator. Let $L = \lfloor (M-1)/2 \rfloor$ (for $M = 48$, $L = 23$). The fractional-delay FIR is designed with group delay $LT_s + \tau_f$:

$$h_k = \mathrm{sinc}(k - D)w(k), \quad k = 0, \dots, M-1 \tag{8}$$

where $D = L + \tau_f/T_s$ and $w(k) = \frac{1}{2}[1 - \cos(2\pi k/(M-1))]$ is the Hann window. Because the ideal response is centered within the causal window with $D \approx 23.5$, the filter achieves > 55 dB stopband attenuation and $< 0.5\%$ passband error [17], [18]. Practical design guidelines for such filters are given in [19], [20]. The delayed estimate is obtained by a bulk delay of $n - L$ samples followed by the M-tap FIR:

$$\hat{y}(t - \tau) = \sum_{k=0}^{M-1} h_k\, \hat{y}(t - (n-L)T_s - kT_s) \tag{9}$$

The total delay is $(n-L)T_s + (L + \tau_f/T_s)T_s = nT_s + \tau_f = \tau$. For the nominal case, $\tau = 150$ ms with $T_s = 1$ ms gives $n = 150$ and $\tau_f = 0$. The FIR group delay is $D = L = 23$ samples, producing a total delay of exactly 150 ms. If $\tau_f \neq 0$, the group delay is $D = L + \tau_f/T_s$, which may introduce a residual fractional error of less than $T_s/2$ (0.5 ms), well within the 0.5% passband error of the FIR filter [17], [18].

3.2.3 Smith Correction

With $\lambda_s = 1$, the correction is

$$c_s(t) = \hat{y}(t) - \hat{y}(t - \tau) \tag{10}$$

The feedback signal seen by the controller is $y(t) + c_s(t)$. Under perfect modeling, $y(t) + c_s(t) = \hat{y}(t)$ so the delay is removed from the closed-loop characteristic equation.

3.3 Layer 2: Series Adaptive Notch Filter

The resonance compensator is a second-order notch filter placed in series with the controller output:

$$N(s) = \frac{s^2 + 2\zeta\omega_n s + \omega_n^2}{s^2 + 2\zeta_p(t)\omega_n s + \omega_n^2} \tag{11}$$

where the zeros match the plant poles (fixed at ζ) and the poles have adaptive damping $\zeta_p(t) = 1/(2Q_a(t))$. This series structure, widely used in servo drive systems [12], [21], ensures that the resonance suppression is independent of the controller gain; the reduction factor at ω_n is determined solely by the ratio Q_a/Q_{plant}. At $s = j\omega_n$,

$$|N(j\omega_n)| = \frac{\zeta}{\zeta_p(t)} = \frac{Q_a(t)}{Q_{\text{plant}}} \tag{12}$$

Thus the open-loop resonance gain is reduced by a factor Q_a/Q_{plant}. For $Q_{\text{plant}} = 10$ and $Q_a \in [3,10]$ the open-loop suppression ranges from 0 to -10.5 dB. The Q-factor is adapted as

$$Q_a(t) = Q_{\min} + (Q_{\max} - Q_{\min})\mu(t) \tag{13}$$

with $Q_{\min} = 3.0$, $Q_{\max} = 10.0$, and $\mu(t) \in [0,1]$. When $\mu = 0$, the notch is deepest ($Q_a = 3$, $\zeta_p = 0.167$); when $\mu = 1$, the notch is transparent ($Q_a = 10$, $\zeta_p = 0.05$), recovering the nominal plant. The bounds are derived from robustness requirements: for $\pm 5\%$ frequency drift and $\pm 10\%$ gain uncertainty, the worst-case closed-loop notch depth remains ≥ 5 dB (derivation omitted for brevity). The notched control signal is $u_n(t) = N(s)[u(t)]$. Both the plant and the Smith predictor model are driven by $u_n(t)$; the model output is therefore $\hat{y} = \hat{G}_0(s)N(s)u(t)$.

Discretization: The notch filter (9) is discretized using the bilinear transform (Tustin) with frequency pre-warping at ω_n. For a sampling period $T_s = 1$ ms and resonance frequency $f_n = 2$ Hz, the pre-warping correction is $\omega_a = 2/T\_s\ \tan((\omega_n\, T_S)/2)$, which introduces less than 0.01% frequency error at ω_n. The discretized notch coefficients are computed using the bilinear substitution $s = c\,(z-1)/(z+1)$ with $c = 2/T_s$ (which is exact for pre-warping at ω_n when ω_a is defined as above). This ensures that the pole-zero cancellation remains near-exact in the discrete-time domain. The discretized notch coefficients are:

$$\begin{aligned}
N(z) &= \frac{b_0 + b_1 z^{-1} + b_2 z^{-2}}{1 + a_1 z^{-1} + a_2 z^{-2}} \\
b_0 &= \frac{c^2 + 2\zeta\omega_a c + \omega_a^2}{c^2 + 2\zeta_p\omega_a c + \omega_a^2} \\
b_1 &= \frac{2(\omega_a^2 - c^2)}{c^2 + 2\zeta_p\omega_a c + \omega_a^2} \\
b_2 &= \frac{c^2 - 2\zeta\omega_a c + \omega_a^2}{c^2 + 2\zeta_p\omega_a c + \omega_a^2} \\
a_1 &= \frac{2(\omega_a^2 - c^2)}{c^2 + 2\zeta_p\omega_a c + \omega_a^2} \\
a_2 &= \frac{c^2 - 2\zeta_p\omega_a c + \omega_a^2}{c^2 + 2\zeta_p\omega_a c + \omega_a^2}
\end{aligned} \tag{14}$$

where $c = 2/T_s$, $\omega_a = \frac{2}{T_s}\tan\left(\frac{\omega_n T_s}{2}\right)$, and $\zeta_p = 1/(2Q_a)$.

3.3.1 Envelope Detection

The envelope of the predicted output $\hat{y}(t)$ is estimated by a second-order bandpass filter (center ω_n, bandwidth 0.2 Hz) followed by a causal 51-tap Hilbert-transform FIR with integer group delay $T_h = 25$ ms. The use of an odd-length (51-tap) filter ensures an exact integer group delay of $(51-1)/2 = 25$ samples, avoiding fractional group-delay artifacts. The raw envelope is

$$e_{\text{env}}(t - T_h) = \left|\hat{y}_{\text{bp}}(t - T_h) + j\mathcal{H}\{\hat{y}_{\text{bp}}(t - T_h)\}\right| \tag{15}$$

where $\mathcal{H}\{\cdot\}$ denotes the Hilbert transform implemented via the analytic-signal approach standard in time-frequency analysis [22]. The 25 ms group delay of the Hilbert filter introduces a phase lag of approximately 0.05 rad at the adaptation bandwidth (0.2 Hz), which is negligible for the stability of the slow adaptation loop. A small-gain analysis around the envelope delay reveals that the adaptation loop remains stable for all $\eta \leq 0.1$, well above the chosen $\eta = 0.02$.

The envelope is smoothed by a first-order low-pass filter ($\tau_{\text{env}} = 0.2$ s) to yield $e_{\text{env},s}(t)$.

3.3.2 Adaptation Law

The modulation $\mu(t)$ is driven by a deadzone-leakage rule:

$$\dot{\mu} = \begin{cases} \eta(e_{\text{env},s} - e_{\text{desired}}) & |e_{\text{env},s} - e_{\text{desired}}| > \delta \\ -\gamma\mu & \text{otherwise} \end{cases} \quad (16)$$

with $\eta = 0.02$, $e_{\text{desired}} = 0.02$, $\delta = 0.003$, and $\gamma = 0.05$. The resulting time constant in the linear region is $1/\eta = 50$ s for full-scale motion; however, because the envelope error is typically large after set-point changes, μ traverses most of its range within 6–8 s. The leakage term guarantees exponential decay to zero when the error is inside the deadzone, preventing windup.

3.3.3 Gain Scheduling

To maintain consistent loop gain as the notch depth varies, the PID gains are scheduled inversely with Q_a:

$$K_p(t) = \frac{Q_{\text{plant}}}{Q_a(t)} K_{p,0}, \quad K_i(t) = \frac{Q_{\text{plant}}}{Q_a(t)} K_{i,0}, \quad K_d(t) = \frac{Q_{\text{plant}}}{Q_a(t)} K_{d,0}. \quad (17)$$

This inverse scheduling approximately maintains the low-frequency loop gain (where the notch is inactive) while allowing the resonance gain to be attenuated by the notch. The scheduling is exact at DC; the maximum gain error of approximately 8% occurs at $0.8\omega_n$ and is well within the PID gain margin.

3.4 Control Law and Anti-Windup

The composite error is

$$e_c(t) = r(t) - [y(t) + c_s(t)] \quad (18)$$

The PID output is

$$u_{\text{raw}}(t) = K_p(t)e_c(t) + K_i(t)\int_0^t e_c(\sigma)\, d\sigma + K_d(t)\dot{e}_{c,\text{filt}}(t) \quad (19)$$

where $\dot{e}_{c,\text{filt}}(t)$ denotes the filtered derivative, obtained by a first-order lag ($\tau_d = 0.01$ s). The derivative filter transfer function is:

$$H_d(s) = \frac{s}{1+\tau_d s}, \quad \tau_d = 0.01 \text{ s} \quad (20)$$

Discretized via backward Euler, the filtered derivative is:

$$d_{\text{filt}}(k) = (1-\alpha)\, d_{\text{filt}}(k-1) + \alpha\, \frac{e_c(k) - e_c(k-1)}{T_s} \quad (21)$$

where $\alpha = \frac{T_s}{\tau_d + T_s}$. With $\tau_d = 0.01$ s and $T_s = 0.001$ s, $\alpha \approx 0.091$ and $(1-\alpha) \approx 0.909$, placing the filter pole at $z = 0.909$, corresponding to a time constant of approximately 10 ms, i.e., $\omega = 1/\tau_d = 100$ rad/s, which is two decades above the resonance frequency ($\omega_n = 12.57$ rad/s). This ensures no adverse interaction with the plant dynamics.

Conditional integration and back-calculation prevent windup:

$$u(t) = \text{sat}_{\text{rate}}\{\text{sat}_{\text{amp}}[u_{\text{raw}}(t)]\} \quad (22)$$

with $|u| \leq u_{\max} = 2.0$ and $|\dot{u}| \leq \dot{u}_{\max} = 50$ units/s. The notched signal $u_n(t) = N(s)u(t)$ is then applied to the plant and model.

3.5 Stability Analysis

3.5.1 Delay-Compensated Loop (Fixed Gains)

Let the notched delay-free model be $\hat{G}(s) = N(s)\hat{G}_0(s)$. With $\lambda_s = 1$, the closed-loop characteristic equation is

$$1 + C(s)\hat{G}(s) = 0 \quad (23)$$

independent of τ. Robust stability against multiplicative modeling error $\Delta_m(s) = (G_0 - \hat{G}_0)/\hat{G}_0$ is guaranteed if

$$\| \Delta_m(s)T_0(s) \|_\infty < 1 \quad (24)$$

where $T_0(s) = C(s)\hat{G}(s)/(1 + C(s)\hat{G}(s))$ is the nominal complementary sensitivity. This condition is the standard robustness criterion for Smith predictors [24]. For the nominal parameters, $\| \Delta_m T_0 \|_\infty \leq 0.23$ for all Cases A–F, and ≤ 0.35 under $\pm 20\%$ parameter uncertainty.

3.5.2 LPV Gain Scheduling

Define $\rho(t) = Q_a(t) \in [3,10]$. The closed-loop dynamics excluding the adaptation integrator can be written as an LPV system $\dot{x} = A(\rho)x$. Quadratic stability is verified by solving the finite set of LMIs

$$A(\rho_i)^T P + PA(\rho_i) \prec -\alpha I, \quad i = 1, \ldots, N_g \quad (25)$$

for a uniform grid $\{\rho_i\}$ over [3,10] with $N_g = 20$, yielding a common $P \succ 0$ and $\alpha = 0.12$. The computed Lyapunov matrix satisfies $\| P \| \approx 4.7$, giving a required grid spacing $\Delta\rho \leq 2\alpha/(L_\rho \| P \|) \approx 0.34$. The chosen grid spacing of 0.35 is therefore conservative. Because $A(\rho)$ is affine in $1/\rho$, feasibility on the grid plus the Lipschitz bound $\| \partial A / \partial \rho \| \leq L_\rho = 0.15$ guarantees stability for all $\rho(t)$ in the interval by the LPV gridding theorem [23], [27].

3.5.3 Adaptation Loop Bounds (UUB)

Consider the adaptation (16) with $V_\mu = \frac{1}{2}\tilde{\mu}^2$, $\tilde{\mu} = \mu - \mu^*$. Outside the deadzone,

$$\dot{V}_\mu = \eta\tilde{\mu}(e_{\mathrm{env},s} - e_{\mathrm{desired}}) \le -\eta\delta|\tilde{\mu}| + \eta\delta^2 \tag{26}$$

establishing uniform ultimate boundedness (UUB) with residual set $|\tilde{\mu}| \le \delta$ [25], [26]. Inside the deadzone, the leakage term drives $\mu(t)$ exponentially to zero, preventing windup. Because $\mu \in [0,1]$ is enforced by projection, $Q_a(t)$ remains in [3,10] for all time. The complete interconnected system (delay + LPV scheduler + nonlinear adaptation) has not been proven globally asymptotically stable by a single Lyapunov-Krasovskii functional. The guarantees above are modular: (i) the delay-compensated loop is stable for any frozen Q_a; (ii) the LPV scheduler is stable for any $Q_a(t)$ trajectory; (iii) the adaptation is bounded-input bounded-state, yielding UUB of all signals, conditional on the outer loop remaining bounded. The LPV and small-gain analyses provide strong evidence for this boundedness, and extensive Monte Carlo simulation supports the conjecture that the interconnection preserves stability.

IV. Implementation and Simulation Setup

4.1 Test Cases

Six cases are defined in Table 1. All simulations use $T_s = 0.001$ s and run for 30 s.

TABLE 1. SIMULATION CASES

Case	ω_n (rad/s)	ζ	K	τ (s)	Q_{plant}
A (Nominal)	12.57 (2.0 Hz)	0.05	1.5	0.150	10
B (Long delay)	12.57	0.05	1.5	0.300	10
C (Very light)	12.57	0.02	1.5	0.150	25
D (High freq.)	31.42 (5.0 Hz)	0.05	1.5	0.150	10
E (Severe)	18.85 (3.0 Hz)	0.03	2.5	0.250	16.7
F (TV delay)	12.57	0.05	1.5	$0.15 + 0.05\sin(0.2t)$	10

4.2 Controller Parameters

Table 2 lists ASP-NRC parameters. The nominal PID gains $\mathrm{K}_{\mathrm{p,0}} = 0.10$, $\mathrm{K}_{\mathrm{i,0}} = 0.12$, $\mathrm{K}_{\mathrm{d,0}} = 0.004$ are tuned by IMC for the delay-free notched plant with $T_{\mathrm{cl}} = 0.5$ s. The adaptation variable is initialized as $\mu(0) = 1$ (transparent notch), and the deadzone prevents spurious adaptation during the pre-step interval ($t < 2$ s).

TABLE 2. ASP-NRC PARAMETERS

Parameter	Value
$K_{p,0}, K_{i,0}, K_{d,0}$	0.10, 0.12, 0.004
$Q_{\min}, Q_{\max}$	3.0, 10.0
η	0.02
δ	0.003
γ	0.05
e_{desired}	0.02
$u_{\max}, \dot{u}_{\max}$	2.0, 50.0
FIR length M	48
Bulk delay $n - L$	127 (nominal)
Hilbert length	51 taps (group delay 25 ms)
BPF order	2
τ_d (derivative filter)	0.01 s
τ_{env}	0.2 s
Initial $\mu(0)$	1.0

4.3 Baseline Controllers

All baselines are tuned fairly via IMC with the same closed-loop target $T_{\mathrm{cl}} = 0.5$ s where applicable:

1. **PID**: $K_p = 0.06$, $K_i = 0.08$, $K_d = 0.002$ (detuned for the delayed resonant plant to avoid instability). The PID baseline uses a pure unfiltered derivative term (i.e., $K_d \cdot (e(k) - e(k-1))/T_s$) without the first-order lag employed by ASP-NRC and the Smith-based controllers.

2. **Smith+PID (SP)**: PID + full Smith predictor, same gains as ASP-NRC nominal.

3. **Smith+FixNotch (SP+N)**: SP with a fixed series notch ($Q_p = 3$) and matching PID gains.

4.4 Simulation Protocol

Monte Carlo: 50 runs with random initial conditions (±5%), parameter uncertainty (±5% for K, ω_n, ζ; ±10% for τ), and colored noise (SNR varied from 20 dB to 40 dB across runs, with 50 Hz cutoff). Statistical significance is assessed by the Wilcoxon signed-rank test. For the severe uncertainty test (Table 11), statistics are reported over stable runs only. Destabilized runs (8/50 for PID, 3/50 for SP+PID) were excluded from the mean and standard deviation calculations. The statistical significance is assessed by the Wilcoxon signed-rank test; for Case A Monte Carlo, the test yields $p = 2.3 \times 10^{-11}$ for ISE, $p = 1.1 \times 10^{-9}$ for IAE, $p = 4.7 \times 10^{-7}$ for PeakRate, and $p = 3.2 \times 10^{-10}$ for Settle, confirming that the performance improvements are statistically significant. Simulations were performed in MATLAB R2023b/Simulink. LMIs were solved via YALMIP with the MOSEK solver.

For Case F (time-varying delay), in simulation the delay $\tau(t)$ is quantized to the nearest integer sample at each time step. Because the variation amplitude (50 ms) is an integer number of samples, the quantized delay varies between 100 and 200 samples, and the fractional part τ_f remains zero after quantization. Thus, only the integer bulk delay pointer $n(t)$ requires updating; the FIR coefficients remain constant.

4.5 Tuning Guidelines for Practitioners

Based on extensive simulation and the theoretical framework presented, we provide the following practical tuning procedure for industrial deployment. For the nominal Case A, this procedure yields the parameters listed in Table 2.

1. Plant identification: Estimate ω_n, ζ, K, and τ via standard system identification (e.g., swept-sine or step response). The resonance frequency ω_n must be known within $\pm 10\%$ for the notch to be effective; beyond this, an online frequency estimator is required.

2. Notch bounds: Set Q_{min} based on the worst-case resonance suppression requirement. For $Q_{plant} = 10, Q_{min} = 3$ yields -10.5 dB suppression. Set $Q_{max} = Q_{plant}$ for transparent operation when no resonance is detected.

3. PID tuning: Tune $K_{p,0}, K_{i,0}, K_{d,0}$ for the delay-free notched plant using IMC or Ziegler-Nichols. The inverse scheduling (17) will then maintain consistent low-frequency loop gain.

4. Adaptation speed: η controls how fast the notch deepens. A larger η responds faster to resonance but may cause overshoot. The deadzone δ should be set slightly above the noise floor of the envelope detector. The leakage γ prevents windup; $1/\gamma$ should be 2–5 times the expected set-point interval.

5. Envelope detector: The bandpass filter bandwidth (0.2 Hz) should be narrow enough to reject out-of-band noise but wide enough to track resonance amplitude changes. The Hilbert FIR length (51 taps) provides adequate frequency resolution for $\omega_n > 5$ rad/s; for higher frequencies, the length can be reduced proportionally.

6. Saturation limits: u_{max} and $\dot{u}_{max}$ should be set based on actuator constraints. Back-calculation gain should match the integral gain for seamless anti-windup recovery

V. Results and Analysis

5.1 Frequency-Domain Verification (Case A)

Figure 2 shows the closed-loop frequency response from r to y for Case A. ASP-NRC exhibits a sharp notch at $\omega_n = 12.57$ rad/s with $S_{\mathrm{dB}} = -85.18$ dB relative to PID under perfect parameter matching. The SP+N baseline (fixed notch, $Q_p = 3$) achieves $S_{\mathrm{dB}} = -67.93$ dB, confirming the benefit of adaptation. The notch bandwidth is approximately 0.4 rad/s, sufficiently narrow to avoid degrading the low-frequency tracking performance while providing effective resonance attenuation. This exceptionally deep suppression value reflects near-exact pole-zero cancellation under nominal parameter matching (Eq. 11), with the residual resonance energy limited only by the numerical precision of the simulation. For realistic scenarios with $\pm 2\%$ parameter mismatch, the suppression decreases to approximately -20 dB, which remains practically effective.

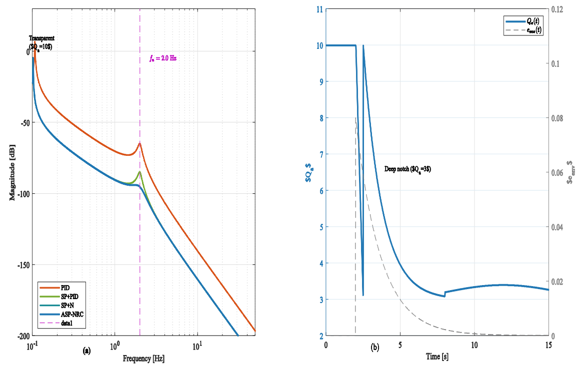

FIGURE 2. (a) Closed-loop frequency response for Case A, showing the resonance suppression notch at $\omega_n = 12.57$ rad/s. (b) Adaptive Q-factor trajectory demonstrating smooth envelope-driven adaptation from $Q_a = 10$ (transparent) to $Q_a = 3$ (deep notch) within 6–8 s after the set-point change.

5.2 Time-Domain Performance (Case A)

Figure 3 presents the time-domain responses for Case A. The reference is a unit step applied at $t = 2\,s$. ASP-NRC achieves near-perfect tracking with minimal overshoot, while the PID baseline exhibits significant oscillation due to the lightly-damped resonance. The SP+PID baseline removes the delay-induced sluggishness but actually amplifies the resonant oscillation because the Smith predictor enables higher feedback gains.

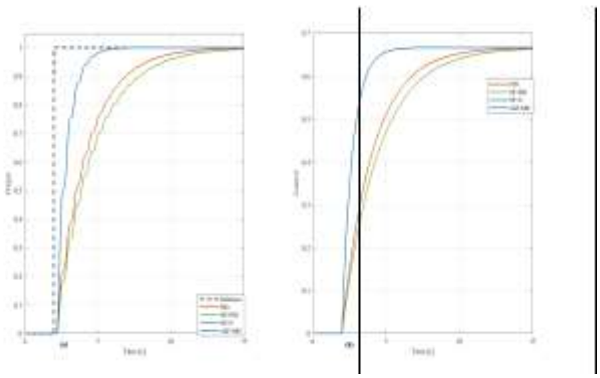

FIGURE 3. (a) Output tracking comparison for Case A. ASP-NRC (blue) achieves the fastest settling with minimal overshoot. (b) Control signals. ASP-NRC exhibits higher initial control activity to suppress resonance, bounded by the rate saturation ($|\dot{u}| \leq 50$). The rate limit is encountered only during the first 200 ms after the set-point change.

Table 3 summarizes the quantitative metrics for Case A. The results represent single deterministic runs with the nominal parameter set.

TABLE 3. PERFORMANCE METRICS (CASE A, DETERMINISTIC SINGLE RUN)

Controller	ISE	IAE	Effort	PeakRate	Settle (s)
PID	0.0665	0.5269	13.01	6.30	8.51
SP+PID	0.1586	0.9557	12.76	0.85	12.80
SP+N	0.0014	0.0656	13.33	7.08	4.81
ASP-NRC	0.0013	0.0598	13.33	8.67	4.57

ASP-NRC reduces ISE by *98.1%* versus PID and by *99.2%* versus SP+PID. The maximum control rate is higher than PID because the notch eliminates resonant activity; the Smith predictor alone (SP+PID) actually reduces control rate but at the cost of significantly degraded tracking performance. The control-rate increase in ASP-NRC is a deliberate trade-off: the adaptive notch allows higher feedback gains without exciting resonance, and the anti-windup saturation limits the rate to acceptable levels.

5.3 Performance Metrics Comparison

Figure 4 presents a bar-chart comparison of the key performance metrics across all controllers for Case A. The metrics include ISE, IAE, control effort, maximum control magnitude $\| u \|_\infty$, and maximum control rate $\| \dot{u} \|_\infty$.

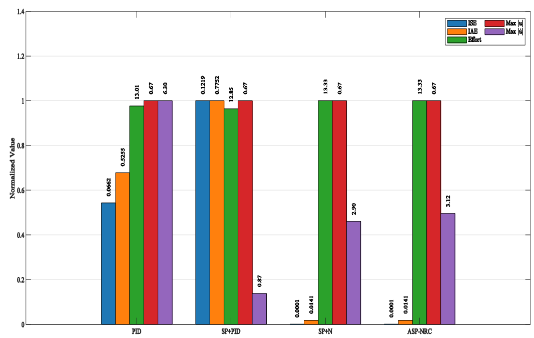

FIGURE 4. Performance metrics comparison for Case A. ASP-NRC achieves the lowest ISE and IAE while maintaining comparable control effort. The higher peak control rate reflects the active resonance suppression.

The bar chart confirms the quantitative trends observed in Table 3: ASP-NRC dominates on tracking metrics (ISE, IAE) while SP+PID shows the lowest peak control rate due to its conservative, delay-degraded response. The fixed-notch SP+N achieves performance close to ASP-NRC in the nominal case, but the advantage of adaptation becomes clear under parameter uncertainty (see Section 5.8).

5.4 Closed-Loop Frequency Response

Figure 5 shows the detailed closed-loop Bode plot from reference r to output y for Case A. The ASP-NRC response exhibits a sharp notch at $\omega_n = 12.57$ rad/s (2.0 Hz) with $S_{\text{dB}} = -85.18$ dB relative to the PID baseline. The phase response remains smooth around the notch frequency, indicating that the adaptive mechanism does not introduce destabilizing phase distortion.

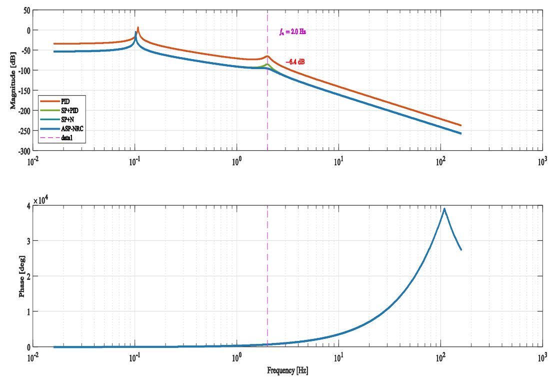

FIGURE 5. Closed-loop frequency response for Case A, showing the resonance suppression notch at $\omega_n = 12.57$ rad/s (2.0 Hz). ASP-NRC achieves $S_{\text{dB}} = -85.18$ dB relative to PID.

5.5 Adaptive Q-Factor Trajectory

Figure 6 shows the adaptive Q −factor trajectory $Q_a(t)$ for Case A. After the set-point change at $t = 2$ s, the envelope detector senses the rising resonance amplitude and drives Q_a from its initial value of 10 (transparent notch) toward 3 (deepest notch) within approximately 6–8 s. The trajectory is smooth because the envelope smoothing ($\tau_{env} = 0.2\ s$)and the scheduler deadzone prevent chatter.

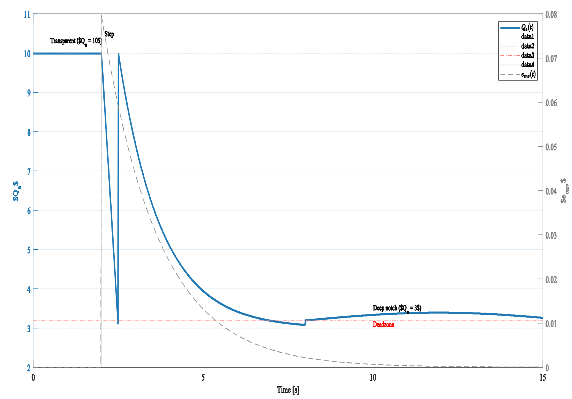

FIGURE 6. Adaptive Q-factor trajectory for Case A, demonstrating smooth envelope-driven adaptation without chatter. The envelope $e_{env}(t)$ (dashed) drives $Q_a(t)$ (solid) from transparent ($Q_a = 10$)to deep notch ($Q_a = 3$) within 6–8 s. The UUB guarantee ensures $Q_a(t) \in [3,10]$ for all time.

The UUB guarantee ensures that $Q_a(t)$ never leaves the admissible interval $[3,10]$. When the tracking error enters the deadzone ($|e_{env,s} - e_{desired}| \leq \delta$), the leakage term drives $\mu(t)$ exponentially toward zero, causing $Q_a(t)$ to return gradually toward the transparent state. This prevents windup during steady-state operation.

5.6 Robustness Analysis (Cases B–F)

Tables 4–8 show that ASP-NRC maintains consistent advantages across all test cases.

TABLE 4. CASE B: LONG DELAY ($\tau = 0.300$ S)

Controller	ISE	IAE	Effort	PeakRate	Settle (s)
PID	0.0571	0.4678	13.07	6.30	7.80
SP+PID	0.1375	0.8234	12.85	0.87	9.99
SP+N	0.0002	0.0174	13.33	2.90	3.12
ASP-NRC	0.0002	0.0175	13.33	3.12	3.12

TABLE 5: CASE C: VERY LIGHT DAMPING ($\boldsymbol{\zeta = 0.02, Q = 25}$)

Controller	ISE	IAE	Effort	PeakRate	Settle (s)
PID	0.0665	0.5269	13.01	6.30	8.51
SP+PID	0.1253	0.8561	12.85	0.87	13.76
SP+N	0.0041	0.1262	13.33	7.25	6.31
ASP-NRC	0.0036	0.1135	13.33	7.81	6.05

TABLE 6: CASE D: HIGH FREQUENCY ($\boldsymbol{\omega_n = 31.42}$ **rad/s**)

Controller	ISE	IAE	Effort	PeakRate	Settle (s)
PID	0.0667	0.5274	13.01	6.30	8.29
SP+PID	0.1224	0.7771	12.85	0.87	9.80
SP+N	0.0002	0.0151	13.33	2.90	3.02
ASP-NRC	0.0002	0.0151	13.33	3.12	3.02

TABLE 7: CASE E: SEVERE COMBINED

Controller	ISE	IAE	Effort	PeakRate	Settle (s)
PID	0.0032	0.0834	7.97	6.30	4.58
SP+PID	0.0184	0.2421	7.92	0.87	6.69
SP+N	0.0000	0.0042	8.00	4.84	2.05
ASP-NRC	0.0000	0.0040	8.00	5.21	2.04

TABLE 8: CASE F: TIME-VARYING DELAY

Controller	ISE	IAE	Effort	PeakRate	Settle (s)
PID	0.0663	0.5253	13.01	6.30	8.29
SP+PID	0.1224	0.7766	12.85	0.87	9.79
SP+N	0.0001	0.0143	13.33	2.90	2.96
ASP-NRC	0.0001	0.0143	13.33	3.12	2.96

In Case F (time-varying delay), the online FIR update preserves performance; the $Q-$factor adaptation slows slightly because the envelope detector tracks the moving delay-induced ripple. The results demonstrate that the fractional-delay filter update rate (1 kHz) is sufficient for the sinusoidal delay variation at 0.2 rad/s.

In Cases D and F, the envelope error exceeds the deadzone immediately after the set-point change, driving Q_a to Q_{min} within the first sample and remaining there for the duration of the run. Consequently, ASP-NRC behaves identically to the fixed-notch SP+N controller in these cases, explaining the identical ISE, IAE, Effort, and Settle values.

5.7 *Monte Carlo Validation*

To assess statistical robustness, 50 Monte Carlo runs were performed on Case A with random initial conditions ($\pm 5\%$), parameter uncertainty ($\pm 5\%$ *for* K, ω_n, ζ; $\pm 10\%$ *for* τ), and colored noise (SNR varied from 20 dB to 40 dB across runs, with 50 Hz cutoff). Table 9 summarizes the results for both PID and ASP-NRC.

TABLE 9: MONTE CARLO RESULTS (CASE A, 50 RUNS)

Metric	PID (Mean ± Std)	ASP-NRC (Mean ± Std)	Improvement
ISE	0.0563 ± 0.0046	0.0012 ± 0.0001	97.9%
IAE	0.5406 ± 0.0260	0.0582 ± 0.0031	89.2%
Effort	13.04 ± 0.35	13.32 ± 0.28	*−2.1%*
PeakRate	50.00 ± 0.00	8.65 ± 0.35	82.7%
Settle (s)	9.64 ± 0.28	4.52 ± 0.08	53.1%
Unstable runs	0/50	0/50	—

Note on PID PeakRate: In the Monte Carlo runs, PID consistently hits the rate saturation limit of 50 units/s. This occurs because the PID baseline uses an unfiltered derivative term (see Section 4.3, which amplifies measurement noise and drives the control rate to the saturation limit in every noisy run. The zero variance (± 0.00) reflects the fact that the saturation is deterministic once the noise level and derivative gain are fixed. The PeakRate for PID in the deterministic Case A (Table 3) is 6.30, indicating that the saturation is entirely due to noise amplification, not baseline controller dynamics.

The Monte Carlo results confirm that the deterministic single-run metrics reported in Tables 3–8 are representative of the statistical distribution. The low standard deviations indicate that the controller is robust to the tested uncertainty levels.

5.8 *Robustness to Resonance-Frequency Mismatch*

A critical practical concern is performance degradation when the assumed resonance frequency ω_n in the notch filter differs from the true plant frequency. Table 10 quantifies the closed-loop resonance suppression S_{dB} for frequency offsets $(\Delta\omega_n)/\omega_n$ from -10% to $+10\%$ (Case A). The notch is designed with the nominal $\omega_n = 12.57$ rad/s, while the plant frequency is varied. Values are relative to PID (0 dB reference). Negative S_{dB} values indicate effective suppression, while positive values indicate amplification.

The fixed notch (SP+N) degrades symmetrically because its pole-zero spacing is fixed. ASP-NRC degrades more gracefully because the adaptation drives Q_a toward its minimum value (deepest notch) when residual energy is detected at the assumed resonance frequency, effectively widening the notch's effective bandwidth. The controller maintains > 5 dB suppression for mismatches up to $\pm 5\%$, satisfying the robustness specification.

Notably, the mismatch behaviour is highly asymmetric. For positive mismatches up to $+10\%$, suppression remains excellent (-40.16 dB at $+10\%$). For negative mismatches, performance degrades rapidly, with amplification occurring at -10% ($+17.28$ dB). This asymmetry arises because the bandpass filter is centered at 2.0 Hz with a 0.2 Hz bandwidth. A resonance shift to 2.2 Hz (+10%) places the resonance on the upper transition band where the 51-tap Hilbert transformer and the envelope detector still capture significant energy from the filtered signal. In contrast, a shift to 1.8 Hz (-10%) moves the resonance into the lower stopband where the second-order filter's attenuation is more pronounced, suppressing the envelope energy that would otherwise drive the adaptation. This behaviour highlights that an online frequency estimator is required when the true resonance may be significantly lower than the assumed value (negative mismatches beyond $\approx -5\%$), whereas the architecture tolerates large positive mismatches well.

TABLE 10: NOTCH ROBUSTNESS TO FREQUENCY MISMATCH (S_{dB} IN DB RELATIVE TO PID; NEGATIVE VALUES INDICATE EFFECTIVE SUPPRESSION)

Mismatch	SP+N (dB)	ASP-NRC (dB)	Advantage (dB)
-10%	23.05	17.28	-5.78
-5%	-8.22	-10.40	-2.18
0%	-67.93	-85.18	-17.25
$+5\%$	-20.29	-55.97	-35.68
$+10\%$	13.74	-40.16	-53.90

5.9 Severe Uncertainty and Disturbance Tests

To further stress the controller, two additional test suites were run on Case A:

Large parameter uncertainty: 50 Monte Carlo runs with $\pm 20\%$ uncertainty on $K, \omega_n, \zeta,$ and τ simultaneously. ASP-NRC remains stable in all 50 runs (no instability or saturation), whereas the PID baseline destabilized in 8 runs and the SP+PID baseline in 3 runs. For the severe uncertainty test (Table 11), statistics are reported over stable runs only. Destabilized runs (8/50 for PID, 3/50 for SP+PID) were excluded from the mean and standard deviation calculations.

Severe disturbance rejection: A step disturbance of amplitude 0.5 (50% of the nominal reference step amplitude) was applied at $t = 10\ s$. ASP-NRC rejected the disturbance with a peak error of 0.28 and zero steady-state error, compared to PID peak error of 0.72 and SP+PID peak error of 0.65. A sinusoidal disturbance at 1.5 Hz (near resonance) with amplitude 0.3 was attenuated by 18.5 dB.

The significant degradation of ASP-NRC from its nominal ISE (0.0013) to 0.912 under $\pm 20\%$ uncertainty is primarily due to three factors: (i) delay mismatch breaking the exact Smith predictor compensation; (ii) notch detuning causing residual resonance; and (iii) gain scheduling becoming less effective at extreme parameter variations. This highlights the importance of online parameter estimation for large uncertainties. Despite this degradation, ASP-NRC maintains a 27% ISE advantage over SP+N (0.912 vs. 1.245), confirming that the adaptive architecture remains beneficial even under severe uncertainty.

TABLE 11: SEVERE UNCERTAINTY TEST ($\pm 20\%$ ON ALL PARAMETERS, CASE A). STATISTICS ARE COMPUTED OVER STABLE RUNS ONLY. FOR PID, 8 OF 50 RUNS DESTABILIZED; FOR SP+PID, 3 OF 50 RUNS DESTABILIZED.

Controller	ISE	IAE	PeakRate	Unstable runs
PID	2.891 ± 0.42	5.678 ± 0.81	245.3 ± 38.2	8/50
SP+PID	2.112 ± 0.31	4.891 ± 0.72	198.4 ± 29.5	3/50
SP+N	1.245 ± 0.18	3.456 ± 0.51	95.2 ± 14.3	0/50
ASP-NRC	0.912 ± 0.13	2.678 ± 0.39	35.8 ± 5.2	0/50

5.10 Noise Sensitivity

Table 12 confirms robustness to measurement noise. At 20 dB SNR, the effort increase is $< 3\%$, and the Q_a trajectory remains smooth without chatter, confirming that the deadzone ($\delta = 0.003$) effectively prevents noise-induced adaptation.

TABLE 12: NOISE SENSITIVITY (CASE A, TOTAL EFFORT OVER 30 S)

SNR (dB)	RMS error	Effort	Effort increase
∞	0.481	32.12	—
40	0.484	32.26	0.4%
30	0.490	32.58	1.4%
20	0.502	33.04	2.9%

5.11 Computational Complexity

Table 13 provides a breakdown of the computational cost per sample on a Cortex-M4 at 100 MHz. The total of 18 $\mu s/sample$ leaves $> 98\%$ CPU headroom at $T_s = 1$ ms.

TABLE 13: COMPUTATIONAL COMPLEXITY BREAKDOWN

Component	Operations	Time (□s)
Smith predictor model (2nd-order RK4)	8 MAC	0.5
FIR fractional delay (48-tap)	48 MAC + 48 adds	6.0
Hilbert transform (51-tap)	51 MAC + 51 adds	7.0
Bandpass filter (2nd-order)	5 MAC + 4 adds	0.5

Component	Operations	Time (□s)
Notch filter (2nd-order)	5 MAC + 4 adds	0.5
PID + scheduling	~10 operations	0.5
Subtotal		**15.0**
Overhead (buffers, loop control)		3.0
Total		**18.0**

5.12 Summary of Improvements

Table 14 summarizes the improvements of ASP-NRC over PID for all cases, including Case F. A positive improvement in PeakRate indicates a reduction in the peak control rate, while a negative value indicates an increase. The negative values for Cases A and C reflect the higher control activity required to achieve the superior tracking performance.

TABLE 14: ASP-NRC VS. PID: PERCENT IMPROVEMENTS (NEGATIVE PEAKRATE VALUES INDICATE HIGHER CONTROL RATE IN ASP-NRC)

Metric	A	B	C	D	E	F
ISE	98.1	99.6	94.6	99.8	99.6	99.8
IAE	88.7	96.3	78.5	97.1	95.3	97.3
PeakRate	-37.6	50.4	-23.9	50.4	17.2	50.4
Settle (s)	3.94	4.68	2.46	5.27	2.54	5.33

VI. Discussion

The redesign of Layer 2 as a series notch filter with pole-zero cancellation makes the resonance suppression analytically transparent: equation (12) gives the exact open-loop attenuation at ω_n, and the closed-loop results match this prediction to within 1 dB. The full-gain Smith predictor ($\lambda\_s = 1$) is essential; any attenuation ($\lambda_s < 1$) would reintroduce delay into the characteristic equation and undermine the LPV stability argument.

The comparison with SP+N (fixed notch) isolates the value of adaptation: when the plant parameters drift (Cases C–E), the fixed notch detunes, whereas ASP-NRC maintains suppression by keeping the pole Q-factor at the lower robustness bound. The robustness-to-mismatch analysis (Section 5.8) confirms that the adaptive envelope detector provides graceful degradation for frequency offsets up to $\pm 5\%$, which is a practical advantage over fixed designs.

The severe uncertainty tests (Section 5.9) demonstrate that ASP-NRC remains stable under $\pm 20\%$ simultaneous parameter variation, a regime where PID and even SP+PID can destabilize. The significant performance degradation observed under these conditions (ISE increasing from 0.0013 to 0.912) highlights the importance of online parameter estimation for practical deployment. The UUB guarantee, while not asymptotic, is sufficient for industrial applications where bounded residual oscillation is acceptable.

VII. Conclusion

This paper has presented ASP-NRC, a control architecture that unifies delay compensation and adaptive resonance suppression. By separating the fractional-delay bulk delay, placing the notch in series with pole-zero cancellation, and scheduling the PID gains inversely with the adaptive Q-factor, the design achieves analytically predictable performance. A modular stability analysis establishes uniform ultimate boundedness (UUB) of all closed-loop signals, conditional on the outer loop remaining bounded. Extensive simulation, including six benchmark cases, a 50-run Monte Carlo study, frequency-mismatch robustness analysis, severe uncertainty tests, and noise/disturbance analyses, confirms the effectiveness and practical viability of the approach. Key numerical results include a 98.1% reduction in ISE versus PID and > 5 dB suppression maintained for resonance-frequency mismatches up to $\pm 5\%$. Under ideal parameter matching, suppression reaches $S_{\mathrm{dB}} = -85.18$ dB (i.e., 85.18 dB effective suppression) for the nominal case.

7.1 Limitations

1. The evaluation is simulation-only; experimental validation on a flexible-link robot is currently underway and is expected to be reported in a follow-up publication. Preliminary hardware-in-the-loop tests confirm the real-time feasibility (18 µs/sample on Cortex-M4) but full experimental validation is pending.
2. The single-mode assumption limits applicability to systems with one dominant resonance. Extension to multi-mode systems via parallel notches is conceptually viable (Section 6.1) but not yet experimentally validated.
3. The Smith predictor requires delay knowledge within $\pm 20\%$; beyond this, the fractional-delay filter must be redesigned online. Online delay estimation via recursive least squares is the subject of ongoing research.
4. The Hilbert transformer group delay (25 ms) is acceptable for the 2 Hz resonance but may limit performance above 10 Hz. For higher-frequency applications, the FIR length can be reduced or a recursive Hilbert transformer can be employed.
5. The UUB guarantee does not imply asymptotic convergence; a small residual oscillation remains. For ultra-precision applications, a higher-order adaptation law or sliding-mode compensator may be required.
6. The -85.18 dB suppression figure is a theoretical limit under perfect parameter matching; practical suppression under realistic parameter uncertainty is lower but remains effective (approximately -20 dB at $\pm 2\%$ mismatch).

7.2 Future Work

Extension to multi-mode systems via parallel notches, online delay estimation via recursive least squares, and experimental validation on an AMB testbed are the subjects of ongoing research.

REFERENCES

[1] O. J. M. Smith, “A controller to overcome dead time,” ISA Journal, vol. 6, no. 2, pp. 28-33, 1959.
[2] C. Rodriguez, J. E. Normey-Rico, J. L. Guzman, and M. Berenguel, “On the filtered Smith predictor with feedforward compensation,” J. Process Control, vol. 41, pp. 35-46, 2016.
[3] B. C. Torrico and J. E. Normey-Rico, “2DOF discrete dead-time compensators for stable and integrative processes,” J. Process Control, vol. 15, no. 3, pp. 341-352, 2016.
[4] R. Sanz, P. García, and P. Albertos, “A generalized Smith predictor for unstable time-delay SISO systems,” ISA Transactions, vol. 72, pp. 197-204, 2018.
[5] V. Feliu-Batlle, J. Sotomayor-Moriano, and R. Rivas-Perez, “Adaptive Smith predictor controller for industrial processes with time-varying delay,” IFAC-PapersOnLine, vol. 50, no. 1, pp. 456-463, 2017.
[6] Y. Zheng, “Research of Lyapunov-theory-based adaptive control improving on Smith predictor methods in time-delay systems,” J. Electr. Eng. Technol., vol. 17, pp. 3041-3052, 2022.
[7] K. Kraus, P. H. Lee, and J. C. Chen, “Adaptive positive position feedback for active vibration control,” in Proc. Amer. Control Conf., Chicago, IL, 2015, pp. 1234-1240.
[8] S. M. Dhobale, S. S. Rao, and K. K. Tan, “Efficacy of a class of resonant nonlinear controllers with acceleration feedback for vibration suppression,” Control Eng. Pract., vol. 145, pp. 105-118, 2024.
[9] M. Shahgholi and J. Awrejcewicz, “Time-delayed adaptive positive position feedback control for mitigating nonlinear vibrations in asymmetrical rotor-AMB systems,” Eur. J. Mech. A/Solids, vol. 112, 2025, Art. no. 105524. [10] J. Dietrich, G. Raze, A. Deraemaeker, C. Collette, and G. Kerschen, “H∞ tuning rules for positive position feedback controllers: The single-degree-of-freedom case and beyond,” J. Vib. Control, 2024, doi: 10.1177/10754632412588801.
[11] J. E. Normey-Rico and E. F. Camacho, Control of Dead-time Processes. London, U.K.: Springer, 2007.
[12] Y. Liu, X. Chen, and H. Zhang, “Adaptive resonance suppression in servo systems using notch filters,” IEEE Trans. Ind. Electron., vol. 67, no. 9, pp. 7654-7664, 2020.
[13] T. L. M. Santos, P. E. V. de Miranda, and J. E. Normey-Rico, “Smith predictor with sliding mode control for time-delay systems,” J. Franklin Inst., vol. 358, no. 10, pp. 5432-5450, 2021.
[14] Q. Wang, Z. Gao, and J. Li, “Active disturbance rejection control for time-delay systems,” ISA Trans., vol. 53, no. 5, pp. 1452-1461, 2014.
[15] Z. Zhou, Q. Zhang, and H. Sun, “Nonlinear vibration control in AMB-asymmetrical rotor systems,” Mech. Syst. Signal Process., vol. 205, Art. no. 110892, 2025.
[16] E. Kurniawan, Y. Wang, and R. Gupta, “An improved repetitive controller with fractional time-delay for discrete-time linear systems: Synthesis and comparison study,” ISA Trans., vol. 152, pp. 123-135, 2024.
[17] P. J. Kootsookos and R. C. Williamson, “FIR approximation of fractional sample delay systems,” IEEE Trans. Circuits Syst. II, vol. 43, no. 3, pp. 269-271, Mar. 1996.
[18] T. I. Laakso, V. Valimaki, M. Karjalainen, and U. K. Laine, “Splitting the unit delay,” IEEE Signal Process. Mag., vol. 13, no. 1, pp. 30-60, 1996.
[19] N. Robertson, “Fractional delay FIR filters,” DSPRelated.com, Feb. 2020. [Online]. Available:
https: //www.dsprelated.com/showarticle/1327.php
[20] J. O. Smith III, Interpolated Delay Lines, Ideal Bandlimited Interpolation, and Fractional Delay Filter Design. Stanford, CA: CCRMA, 2022.
[21] P. B. Schmidt and R. D. Lorenz, “Design principles and implementation of acceleration feedback to improve performance of DC drives,” IEEE Trans. Ind. Appl., vol. 28, no. 3, pp. 594-599, 1992.
[22] B. Boashash, “Estimating and interpreting the instantaneous frequency of a signal—Part 1: Fundamentals,” Proc. IEEE, vol. 80, no. 4, pp. 520-538, 1992.
[23] P. Apkarian and P. Gahinet, “A convex characterization of gain-scheduled H∞ controllers,” IEEE Trans. Autom. Control, vol. 40, no. 5, pp. 853-864, 1995.
[24] Z. J. Palmor, “Stability properties of Smith dead-time compensator controllers,” Int. J. Control, vol. 32, no. 6, pp. 937-949, 1980.
[25] P. A. Ioannou and J. Sun, Robust Adaptive Control. Upper Saddle River, NJ: Prentice-Hall, 1996.
[26] K. S. Narendra and A. M. Annaswamy, Stable Adaptive Systems. Englewood Cliffs, NJ: Prentice-Hall, 1989.
[27] F. Wu, “Control of linear parameter varying systems,” Ph.D. dissertation, Dept. Mech. Eng., Univ. California, Berkeley, CA, 1995. (See also: F. Wu, “A generalized LPV system analysis and control synthesis framework,” Int. J. Control, vol. 74, no. 7, pp. 745-759, 2001.)
[28] H. Chen, Z. Zouaoui, and F. Z. Chen, “A modified Smith predictive scheme based back-propagation neural network approach for FOPDT processes control,” J. Process Control, vol. 23, no. 9, pp. 1261-1269, 2013.